PERGAMON

International Journal of Heat and Mass Transfer 42 (1999) 1205–1215

International Journal of HEAT and MASS TRANSFER

Numerical investigation of buoyancy driven flow in a fluid saturated non-Darcian porous medium

P. Nithiarasu[a,*], K. N. Seetharamu[b], T. Sundararajan[c]

[a] *Institute for Numerical Methods in Engineering, University of Wales Swansea, Singleton Park, Swansea SA2 8PP, U.K.*

[b] *School of Mechanical Engineering, Universiti Sains Malaysia, Malaysia*

[c] *Department of Mechanical Engineering, Indian Institute of Technology, Madras, Chennai 600 036, India*

Received 2 October 1997; in final form 21 July 1998

Abstract

The natural convective flow and associated heat transfer in a fluid saturated porous medium have been investigated using the generalised porous medium approach. Many new features have been predicted with the convective heat transfer boundary condition. A detailed parametric study reveals that multicellular flow patterns appear at higher Darcy and Rayleigh numbers and lower Biot numbers. Results are presented for a Darcy number range of 10^{-7}–10^{-2}, Rayleigh number range of 10^{2}–10^{9} and aspect ratios from 1 to 10.

Nomenclature

A aspect ratio (H/L)
Bi Biot number
c_p specific heat
Da Darcy number
g acceleration due to gravity
H height of the porous cavity
h convective heat transfer coefficient
J viscosity ratio
k average thermal conductivity $(\varepsilon k_f + (1-\varepsilon)k_s)$
k^* conductivity ratio (k/k_f)
L characteristic dimension
Nu average Nusselt number
p pressure
Pr Prandtl number
Ra Rayleigh number
T temperature
t time
u, v velocity components
$|\vec{V}|$ total velocity vector
x, y coordinate axes.

Greek symbols
α thermal diffusivity
β coefficient of thermal expansion
ε porosity
κ permeability
ν kinematic viscosity
σ ratio of heat capacities
ρ density.

Subscripts
c cold
f fluid
h hot
s solid
∞ ambient.

1. Introduction

Porous media flows are encountered in a variety of applications such as thermal insulation, underground water flow, oil recovery, etc. Although early work in this area pertained to flow in consolidated porous medium [1–5], more general models have been developed for loosely packed media [5–10]. In particular momentum equations which are similar to the Navier–Stokes equations for free fluid flow has been proposed in recent years [8–10]. Such

* Corresponding author. Fax: 0044 01792 29 5676; e-mail: p.nithiarasu@swansea.ac.uk

0017–9310/98/$ - see front matter
PII: S0017-9310(98)00254-3

models have provided the theoretical tools for analysing physical problems such as alloy solidification, flows over heat exchanger pipes, etc. [11, 12], which can be approximated by an equivalent loosely packed porous medium.

Application of the generalised porous medium model for the analysis of natural convective flow in enclosure filled with a fluid saturated porous medium is of recent origin [10]. Such investigation became particularly relevant in the higher ranges of Rayleigh and Darcy numbers. Very interesting phenomena such as flow channeling near the walls occur for the higher range of *Ra* and *Da* which profoundly influence the nature of the flow and heat transfer processes.

The earlier studies, involving natural convection in porous enclosures, are primarily limited to lower Rayleigh numbers in the non-Darcy flow regimes ($Da > 10^{-4}$). Moreover, a majority of enclosure studies deal with simpler boundary conditions such as prescribed wall temperature and prescribed wall heat flux [1–10]. In the present study, the non-Darcy natural convective flow in a porous cavity is investigated over a wide range of Rayleigh (10^2–10^9) and Darcy numbers (10^{-7}–10^{-2}) with a convective type of heat transfer boundary condition on a vertical wall. The convective boundary condition is especially relevant for conjugate problems where heat exchange occurs between the porous cavity and the medium outside. The present study also focuses attention on the effects of imposed wall heat transfer coefficient and the cavity aspect ratio upon the flow structure and heat transfer.

2. Problem formulation and governing equations

A rectangular cavity filled with fluid saturated porous medium, having insulated horizontal walls and vertical walls, subjected to isothermal and free convective conditions is considered (Fig. 1). The properties with the exception of density are assumed to be constant and the density variation is incorporated through Boussinesq approximation. The generalised set of non-dimensional governing equations for the natural convection flow and heat transfer with uniform porosity are given as:

Continuity equation

$$\frac{\partial u}{\partial x}+\frac{\partial v}{\partial y}=0 \tag{1}$$

x-momentum equation

$$\frac{1}{\varepsilon}\frac{\partial u}{\partial t}+\frac{1}{\varepsilon^2}u\frac{\partial u}{\partial x}+\frac{1}{\varepsilon^2}v\frac{\partial u}{\partial y}=-\frac{\partial p}{\partial x}+\frac{Pr}{\varepsilon}\left[\frac{\partial^2 u}{\partial x^2}+\frac{\partial^2 u}{\partial y^2}\right]-\frac{Pr}{Da}u-\frac{1.75}{\sqrt{150}}\frac{|\bar{V}|}{\sqrt{Da}}\frac{u}{\varepsilon^{3/2}} \tag{2}$$

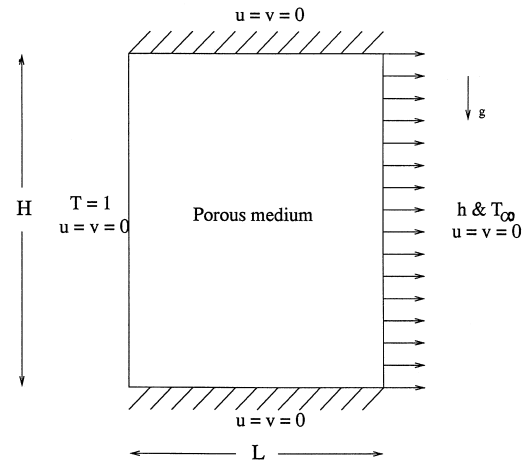

Fig. 1. Buoyancy driven flow in a porous cavity subjected to heat transfer coefficient boundary condition.

y-momentum equation

$$\frac{1}{\varepsilon}\frac{\partial v}{\partial t}+\frac{1}{\varepsilon^2}u\frac{\partial v}{\partial x}+\frac{1}{\varepsilon^2}v\frac{\partial v}{\partial y}=-\frac{\partial p}{\partial y}+\frac{Pr}{\varepsilon}\left[\frac{\partial^2 v}{\partial x^2}+\frac{\partial^2 v}{\partial y^2}\right]-\frac{Pr}{Da}v-\frac{1.75}{\sqrt{150}}\frac{|\bar{V}|}{\sqrt{Da}}\frac{v}{\varepsilon^{3/2}}+RaPrT \tag{3}$$

Energy equation

$$\sigma\frac{\partial T}{\partial t}+u\frac{\partial T}{\partial x}+v\frac{\partial T}{\partial y}=k^*\left(\frac{\partial^2 T}{\partial x^2}+\frac{\partial^2 T}{\partial y^2}\right). \tag{4}$$

The detailed derivation of the governing equations are discussed elsewhere [10]. In the momentum equations (eqns (2) and (3)), the non-linear matrix drag is incorporated through Ergun's correlation [13]. In the governing equations, u and v are volume averaged velocity components; ε is the porosity of the medium and is assumed to be uniform throughout the domain in the present study ($\varepsilon = 0.6$); *Pr* is the Prandtl number; *Ra* is the fluid Rayleigh number; *Da* is the Darcy number; σ is the ratio of heat capacities; T is the nondimensional temperature, k^* is the thermal conductivity ratio and J is the viscosity ratio (this ratio is taken as unity in the present study for the sake of simplicity).

In eqns (2) and (3) the advection terms are also included to entertain porosity values from 0 to 1 [10]. Even though the contribution of this term is small for a porous medium flow, it is included in the model to handle all possible situations including the single phase fluid. Also, from Ref. [14], it is clear that for the smooth development of boundary layer, inclusion of advection terms is necessary.

2.1. Convective heat transfer condition

In the problem considered, the left-side wall of the cavity is subjected to a constant temperature and the right-side wall is exposed to different convective heat transfer coefficients. The temperature scale for this problem is formed in terms of the difference between the prescribed wall temperature and the ambient temperature, which is

$$T = \frac{\bar{T} - T_\infty}{T_h - T_\infty}. \tag{5}$$

The overall heat loss is based on the line integral along the cold wall (right-side wall) of the domain and the relation is:

$$\frac{\partial T}{\partial x} = BiT \tag{6}$$

where Bi is the Biot number defined as:

$$Bi = \frac{hL}{k} \tag{7}$$

with h being the heat transfer coefficient imposed. Other nondimensional parameters used in this study are:

$$x = \frac{\bar{x}}{L}, \quad y = \frac{\bar{y}}{L}, \quad u = \frac{\bar{u}L}{\alpha_f}, \quad v = \frac{\bar{v}L}{\alpha_f}$$
$$p = \frac{\bar{p}\alpha_f}{\rho L^2}, \quad t = \frac{\bar{t}\alpha_f}{L^2}, \quad k^* = \frac{k}{k_f}$$
$$\alpha_f = \frac{k_f}{(\rho c_p)_f}, \quad Pr = \frac{\nu_f}{\alpha_f}, \quad Da = \frac{\kappa}{L^2}, \quad Ra = \frac{g\beta\Delta TL^3}{\nu_f\alpha_f} \tag{8}$$

where the overbar indicates a dimensional quantity.

3. Solution procedure

In the present study, the Galerkin's finite element method is used along with the Eulerian velocity correction procedure. The semi-implicit type of time marching is adopted to accelerate convergence [15, 16]. The velocity correction procedure is well established and available in many research articles [15–17]. The four steps of this scheme can be briefly stated as

1. solve the momentum equations without pressure terms,
2. calculate the pressure from the Poisson equation,
3. correct the velocities, and
4. calculate the temperature field from the energy equation.

The temporal discretisation of Step 1 is given by (calculation of intermediate velocity) [16]:

$$\frac{\tilde{u}^{n+1} - u^n}{\varepsilon\Delta t} = -\frac{3}{2}\left[\frac{u}{\varepsilon^2}\frac{\partial u}{\partial x} + \frac{v}{\varepsilon^2}\frac{\partial u}{\partial y}\right]^n + \frac{1}{2}\left[\frac{u}{\varepsilon^2}\frac{\partial u}{\partial x} + \frac{v}{\varepsilon^2}\frac{\partial u}{\partial y}\right]^{n-1}$$
$$+\left[\frac{Pr}{\varepsilon}\left(\frac{\partial^2\tilde{u}}{\partial x^2} + \frac{\partial^2\tilde{u}}{\partial y^2}\right) - \frac{Pr}{Da}\tilde{u} - \frac{1.75}{\sqrt{150}}\frac{|\bar{V}|}{\sqrt{Da}}\frac{\tilde{u}}{\varepsilon^{3/2}}\right]^{n+1}. \tag{9}$$

The Galerkin's finite element method is used for the spatial discretisation of the above equation. The final matrix form of the discretised equation is given as:

$$\{[M] + \Delta t[K] + \Delta t[D_1] + \Delta t[D_2]\}\tilde{u}_i = [M]u^n + \Delta t\{\{F\} - [A_1]u_i^n + [A_2]u_i^{n-1}\} + \Delta t[G]T^n \tag{10}$$

Similarly, other steps of the algorithm can also be discretised. Further details on the procedure can be found elsewhere [16].

4. Results and discussion

In this section, the results obtained for a wide range of parameters have been presented. To check the accuracy of the present finite element and generalised model, computed temperature distribution in an enclosed axisymmetric porous cavity is compared with the experimental results in Fig. 2. The vertical walls are at constant different temperatures. The radius and aspect ratios are 5.338 and 1, respectively. The particle size and porosity of the medium are taken as 3 mm and 0.3514, respectively [3]. The Darcy number calculated from the particle size, porosity and characteristic dimension is 4.0×10^{-7} and the corresponding Rayleigh numbers to match the Darcy–Rayleigh number of experiment is 2.775×10^8. The conductivity ratio k^* is calculated from the thermal conductivity values of water and glass and is equal to 1.31 for the given porosity and particle size [18]. It is seen that present predictions agree better with the exper-

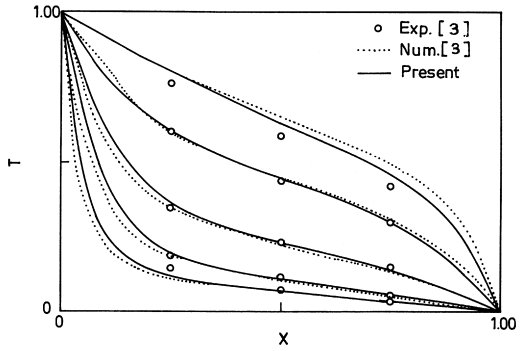

Fig. 2. Comparison of present temperature predictions with the experimental and theoretical predictions in literature, $Da = 4 \times 10^{-7}$, $Ra = 2.775 \times 10^8$, $k^* = 1.31$, $A = 1$.

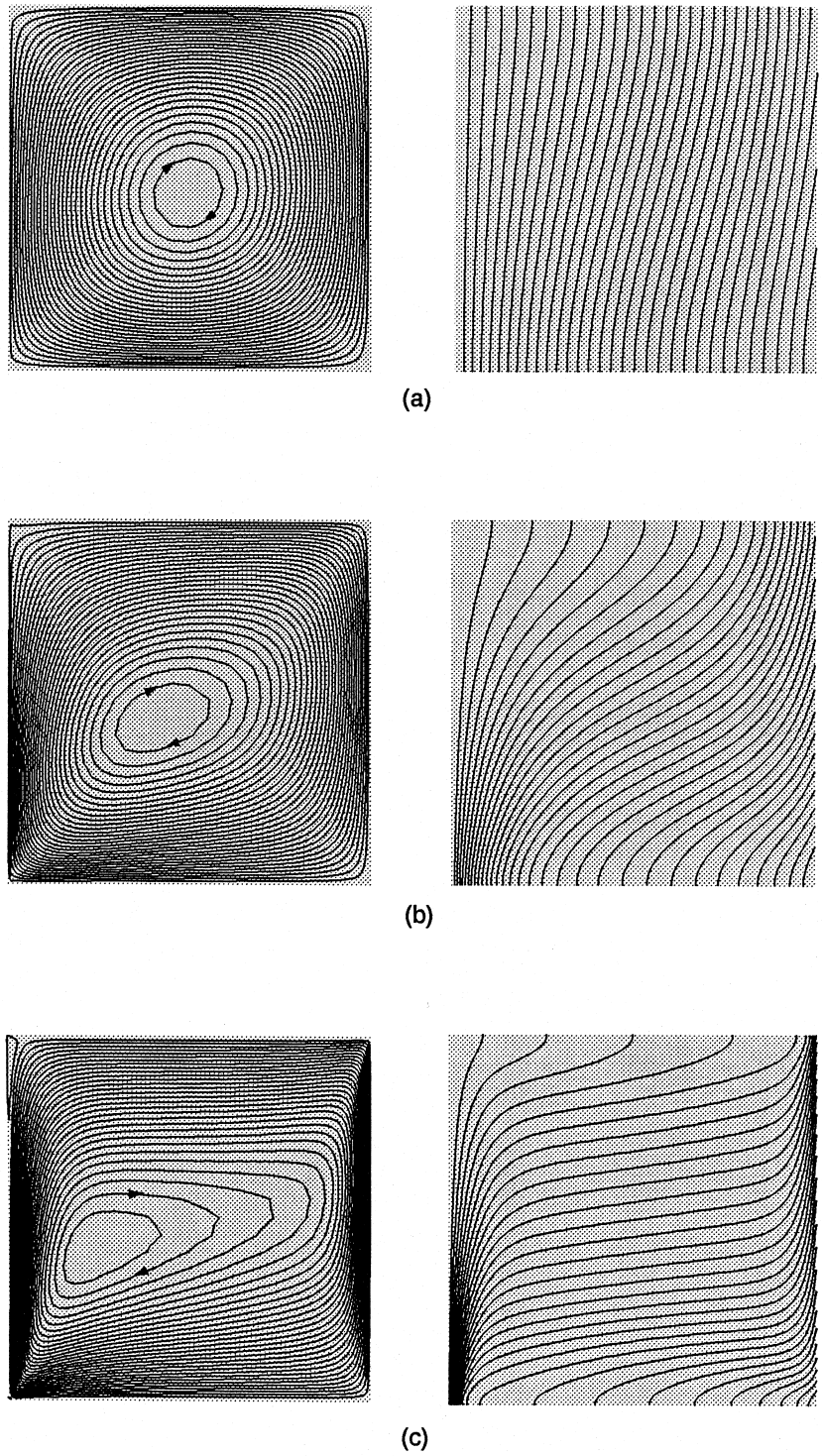

Fig. 3. Flow and isotherm patterns for different Darcy and Rayleigh numbers, $A = 1$: (a) $Da = 10^{-7}$, $Ra = 10^{8}$, $Bi = 2$, $\psi_{max} = 0.476$, $\psi_{min} = -0.001$, $T_{min} = 0.304$; (b) $Da = 10^{-7}$, $Ra = 10^{9}$, $Bi = 2$, $\psi_{max} = 2.715$, $\psi_{min} = -0.025$, $T_{min} = 0.342$; (c) $Da = 10^{-5}$, $Ra = 10^{8}$, $Bi = 10$, $\psi_{max} = 11.607$, $\psi_{min} = 0.0$, $T_{min} = 0.145$.

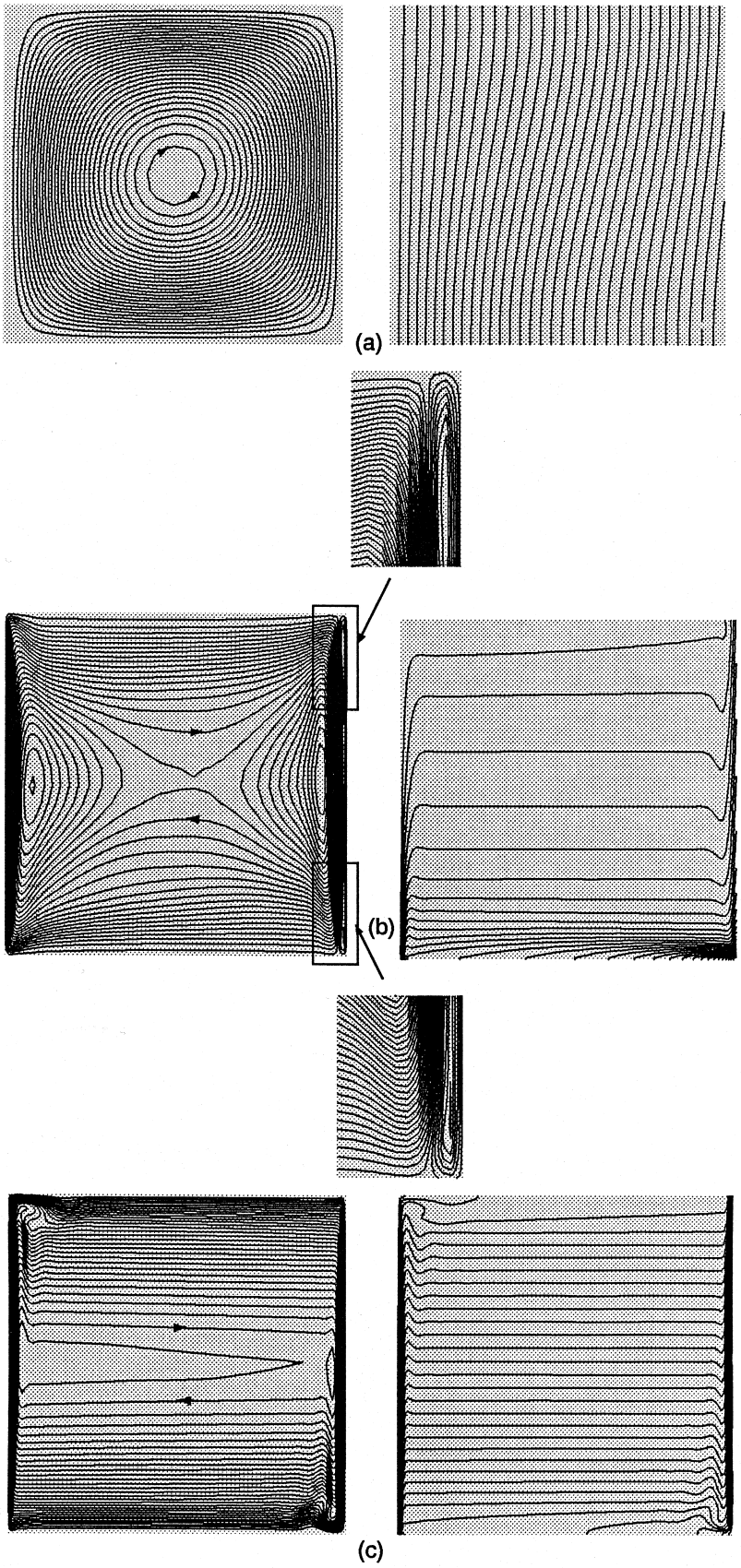

Fig. 4. Flow and isotherm patterns for different Darcy and Rayleigh numbers, $A = 1$: (a) $Da = 10^{-3}$, $Ra = 10^4$, $Bi = 2$, $\psi_{max} = 0.398$, $\psi_{min} = -0.032$, $T_{min} = 0.312$; (b) $Da = 10^{-3}$, $Ra = 10^9$, $Bi = 2$, $\psi_{max} = 31.83$, $\psi_{min} = -1.724$, $T_{min} = 0.627$; (c) $Da = 10^{-3}$, $Ra = 10^9$, $Bi = 500$, $\psi_{max} = 66.561$, $\psi_{min} = 0.0$, $T_{min} = 0.006$.

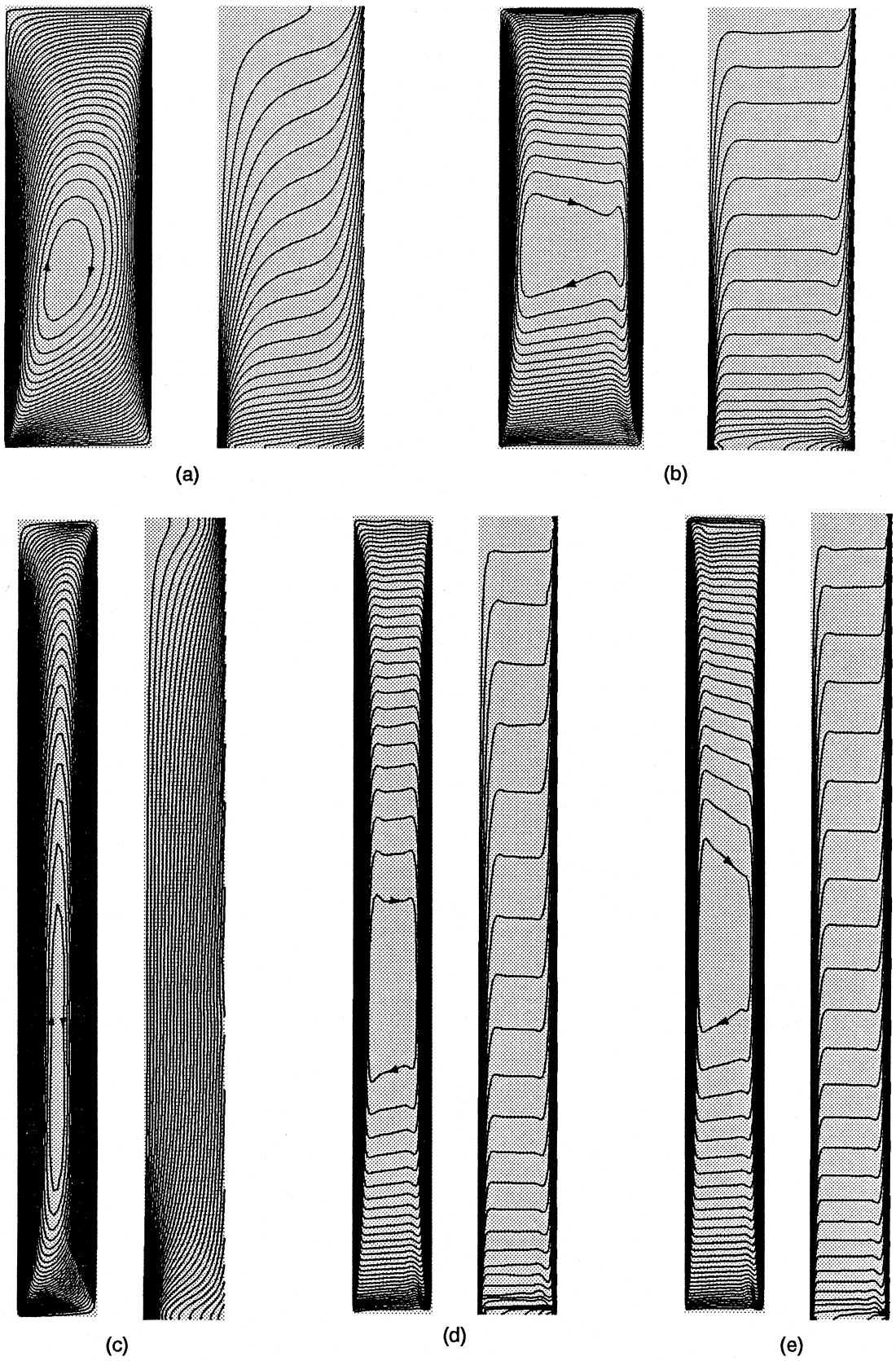

Fig. 5. Flow and isotherm patterns for different aspect ratios: (a) $A = 3$, $Da = 10^{-6}$, $Ra = 10^{9}$, $Bi = 2$, $\psi_{max} = 16.454$, $\psi_{min} = -0.202$, $T_{min} = 0.3478$; (b) $A = 3$, $Da = 10^{-3}$, $Ra = 10^{8}$, $Bi = 1$, $\psi_{max} = 33.03$, $\psi_{min} = -0.18$, $T_{min} = 0.7888$; (c) $A = 10$, $Da = 10^{-6}$, $Ra = 10^{8}$, $Bi = 2$, $\psi_{max} = 7.598$, $\psi_{min} = -0.03$, $T_{min} = 0.1893$; (d) $A = 10$, $Da = 10^{-3}$, $Ra = 10^{8}$, $Bi = 2$, $\psi_{max} = 81.29$, $\psi_{min} = -0.21$, $T_{min} = 0.513$; (e) $A = 10$, $Da = 10^{-3}$, $Ra = 10^{8}$, $Bi = 10$, $\psi_{max} = 112.47$, $\psi_{min} = 0.0$, $T_{min} = 0.1847$.

imental data than the Darcy model results. The comparison of average Nusselt number predictions with experimental data has been given in our earlier publication [10].

Further results are presented for the cavity with convecting cold wall. Here, in addition to the Rayleigh and Darcy numbers, Biot number (non-dimensional heat transfer coefficient) is also varied to study the influences of it upon flow and heat transfer.

Figures 3 and 4 show the flow and isothermal patterns for different Darcy, Rayleigh and Biot numbers. At $Da = 10^{-6}$, the eye of the vortex is observed to move towards the bottom left corner of the cavity with increase in Rayleigh number. At higher Rayleigh numbers, the non-Darcy flow regime (Fig. 4) leads to strong convection motion with boundary layer flow. Also here, at lower Biot numbers, a change in flow pattern occurs with a thin vortex appearing near the cold wall with opposite sense of rotation, for instance, Fig. 4(b) shows such a flow pattern for $Da = 10^{-3}$, $Ra = 10^{9}$ and $Bi = 2$. Further reduction in the Biot number strengthens the additional vortex near cold wall and reduces the heat transfer. The

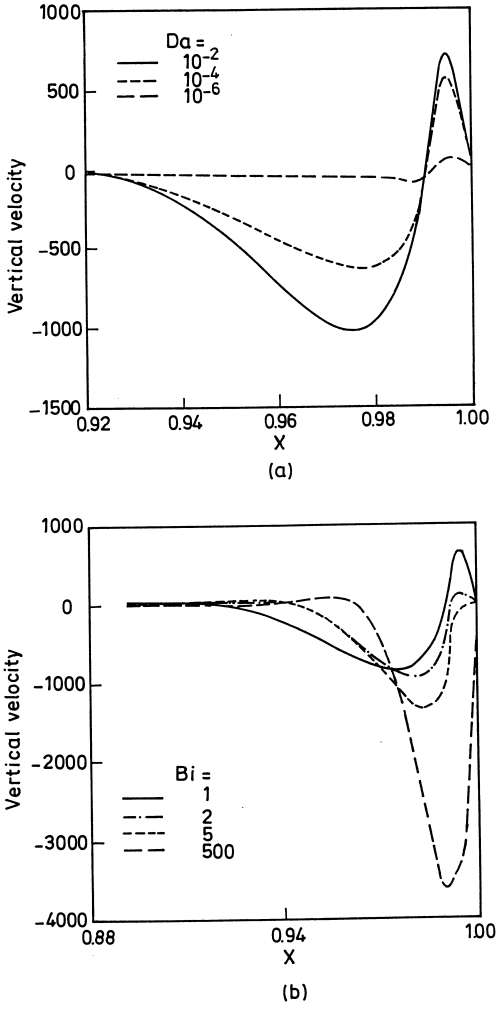

Fig. 6. Vertical velocity distribution near cold wall along the mid-height of the cavity for different Darcy and Biot numbers, $A = 1$: (a) $Da = 10^{-3}$, $Ra = 10^{9}$; (b) $Ra = 10^{9}$, $Bi = 1$.

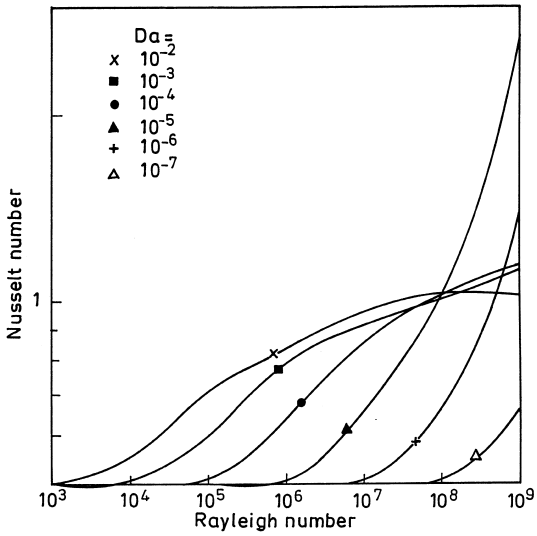

Fig. 7. Average Nusselt number variation with Rayleigh number for different Darcy numbers, $Bi = 1$, $A = 1$.

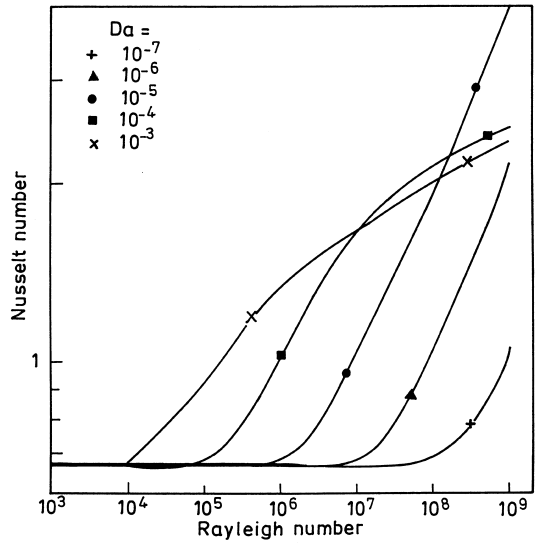

Fig. 8. Average Nusselt number variation with Rayleigh number for different Darcy numbers, $Bi = 2$, $A = 1$.

isotherms of such flow structure at steady state are clustered near the bottom insulated wall. At lower Darcy numbers (in the pure Darcy regime) and at any Rayleigh number considered, no such thin vortices are observed near the cold wall. The thin vortex in the non-Darcy flow regime loses its strength with increase in the Biot number and vanishes at higher Biot numbers (Fig. 4(c)). The appearance of a thin vortex near the cold wall can thus be attributed to the non-Darcian forces and to the insulating effects imposed by the lower heat transfer coefficient on the cold wall. It is also observed that as the Biot number approaches higher values, the flow in both the Darcy and non-Darcy regimes reaches a situation similar to the cavity with isothermal vertical walls (Fig. 4(c)) with strong boundary layer type of flow and channeling near vertical walls.

Streamline and isotherm contours for higher aspect ratios (Fig. 5) follow a similar pattern as observed for square cavity. However, the strength of the counter rotating vortex in the non-Darcy flow regime is rather weak here and is not observed at higher aspect ratios ($A = 10$). Also, here the flow channeling near walls are seen to be quite strong in the non-Darcy flow regime.

Figure 6 shows the vertical velocity distribution near cold wall along the mid-height of a square cavity for different Darcy, Rayleigh and Biot numbers. It is seen at higher Darcy and Rayleigh numbers and lower Biot numbers, that there is a positive velocity distribution near the cold wall. The positive velocity peak approaches negative value with either increase in Biot number or decrease in Darcy number. This prediction is consistent with the observed flow and isothermal patterns (Figs 3 and 4).

Figures 7–10 show the average Nusselt number variation with Rayleigh number for different Darcy and Biot numbers and for an aspect ratio of unity. It is seen that the Nusselt number is a strong function of the Biot number in addition to the Darcy and Rayleigh numbers and it increases with the Biot number. The slopes of the curves are generally less at lower Biot numbers in the non-Darcy flow regime and increases with increase in Biot number. They are observed to be unchanged in the Darcy flow regime and increase with increase in the Biot number. They are observed to be unchanged in the Darcy flow regime with increase in the Biot number. At lower Biot numbers the average Nusselt number curves cross each other at higher Darcy and Rayleigh numbers. This is due to the counter rotating vortex which appears at lower Biot numbers as observed earlier (Fig. 4). Even though the conduction regime is observed for all Biot numbers, the asymptotic and boundary layer flow regimes are not clear at lower Biot numbers due to the counter rotating vortex. As the Biot number increases, the Nusselt number distribution approaches a pattern with different heat transfer regimes as observed for a cavity with isothermal vertical walls (conduction, asymptotic and boundary layer regimes).

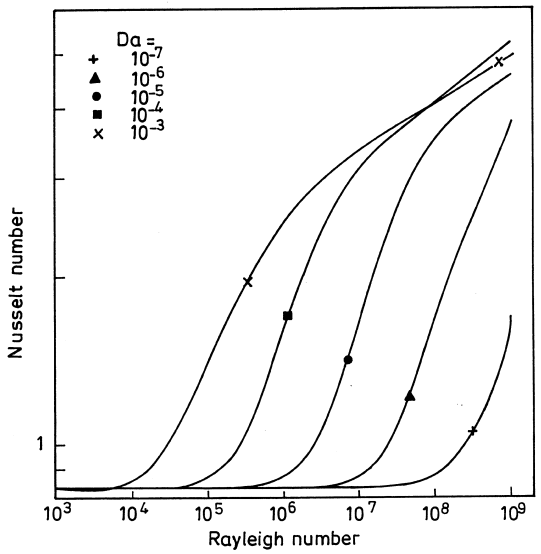

Fig. 9. Average Nusselt number variation with Rayleigh number for different Darcy numbers, $Bi = 5$, $A = 1$.

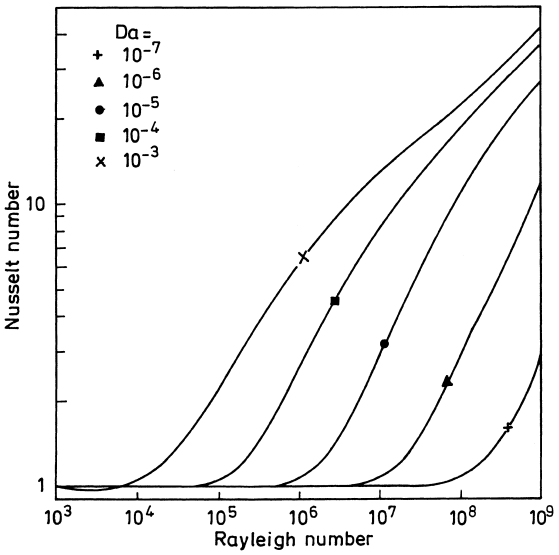

Fig. 10. Average Nusselt number variation with Rayleigh number for different Darcy numbers, $Bi = 500$, $A = 1$.

Average Nusselt number patterns at higher aspect ratios (Fig. 11) are seen to follow the trends observed earlier in the isothermal wall cavities [5]. In this study, the maximum Nusselt number value is obtained near an aspect ratio of about 1 for all the Darcy and Rayleigh numbers considered. In the Darcy flow regime ($Da = 10^{-6}$), the conduction mode dominates up to a Rayleigh number of about 10^7 and a steep increase in the slope is observed as convection starts. At a Darcy number

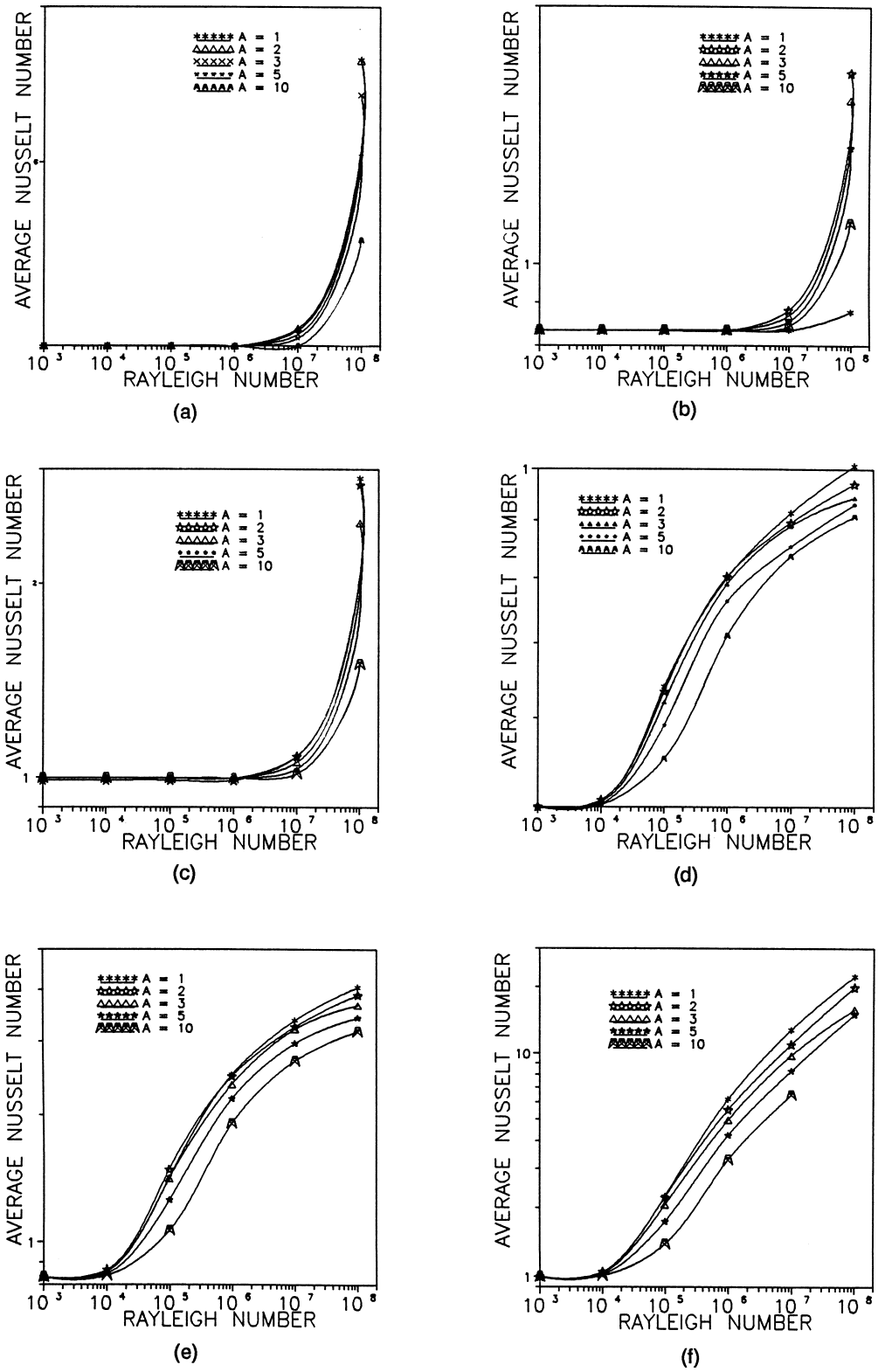

Fig. 11. Average Nusselt number variations with Rayleigh number for different aspect ratios: (a) $Da = 10^{-6}$, $Bi = 1$; (b) $Da = 10^{-6}$, $Bi = 5$; (c) $Da = 10^{-6}$, $Bi = 500$; (d) $Da = 10^{-3}$, $Bi = 1$; (e) $Da = 10^{-3}$, $Bi = 5$; (f) $Da = 10^{-3}$, $Bi = 500$.

of 10^{-3}, the asymptotic regime follows the conduction regime. The rate of heat transfer in the asymptotic regime is higher than that of both conduction and boundary layer regimes.

Figure 12 shows the average Nusselt number distribution with the Biot number for different Darcy and Rayleigh numbers. It is evident from the figure that as the Biot number increases, the Nusselt number approaches a constant value which is almost equal to the case with isothermal vertical walls ($Bi = 500$). At lower Darcy and Rayleigh numbers, the Biot number required to reach this limit is lower than that required at higher Darcy and Rayleigh numbers.

5. Conclusions

Natural convective flow and heat transfer through porous medium have been numerically investigated. The effect of applied heat transfer coefficient on the cold wall of the enclosure upon flow and heat transfer are studied. The differences between the Darcy and non-Darcy flow regimes are clearly brought out through a comprehensive parametric study for different Darcy, Rayleigh and Biot numbers and aspect ratios. The following conclusions are obtained from the study.

A highly convective regime with strong channeling near the walls and higher heat transfer rates have been observed at higher Darcy, Rayleigh and Biot numbers. At lower Biot numbers, a thin vortex with opposite sense of rotation is observed near the cold wall, which vanishes as the Biot number increases. This becomes less strong with a decrease in Darcy number and increase in aspect ratio for the Rayleigh number range considered. The Biot number limit for disappearance of this vortex reduces with decrease in the Darcy number. The slopes of the Nusselt number curves increase with the Biot number in the non-Darcy flow regime and are almost unaltered in the Darcy flow regime. The system approaches a case with isothermal vertical walls as the Biot number increases.

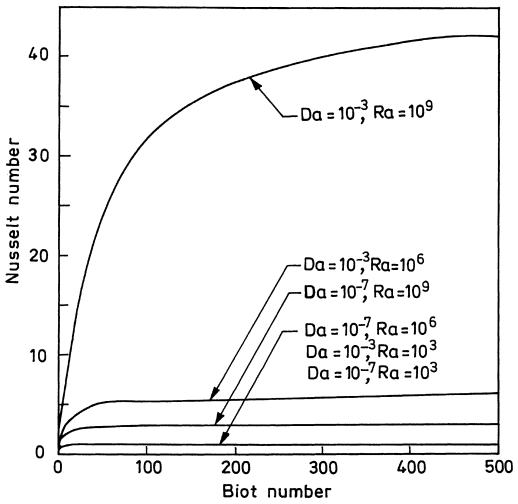

Fig. 12. Average Nusselt number variation with Biot number for different Darcy and Rayleigh numbers, $A = 1$.

References

[1] A. Bejan, On the boundary layer regime in a vertical enclosure filled with a porous medium, Lett. Heat Mass Transfer 6 (1979) 93–102.
[2] B.K.C. Chan, C.M. Ivey, J.M. Barry, Natural convection in enclosed porous media with rectangular boundaries, ASME J. Heat Transfer (1970) 21–27.
[3] V. Prasad, F.A. Kulacki, M. Keyhani, Natural convection in porous media, J. Fluid Mech. 150 (1985) 89–119.
[4] K.L. Walker, G.M. Homsy, Convection in porous cavity, Journal of Fluid Mechanics 87 (1978) 449–478.
[5] V. Prasad, F.A. Kulacki, Convective heat transfer in a rectangular porous cavity—effect of aspect ratio on flow structure and heat transfer, ASME J. Heat Transfer 106 (1984) 158–165.
[6] O.A. Plumb, J.C. Huenefeld, Non-Darcy natural convection from heated surfaces in saturated porous media, Int. J. Heat Mass Transfer 24 (1981) 765–767.
[7] T.W. Tong, E. Subramanian, A boundary layer analysis for natural convection in porous enclosures—use of Brinkman extended Darcy model, Int. J. Heat Mass Transfer 28 (1985) 563–571.
[8] K. Vafai, C.L. Tien, Boundary and inertia effects on flow and heat transfer in porous media, Int. J. Heat Mass Transfer 24 (1981) 195–203.
[9] C.T. Hsu, P. Cheng, Thermal dispersion in a porous medium, Int. J. Heat Mass Transfer 33 (1990) 1587–1597.
[10] P. Nithiarasu, K.N. Seetharamu, T. Sundararajan, Natural convective heat transfer in an enclosure filled with fluid saturated variable porosity medium, Int. J. Heat Mass Transfer 40 (16) (1997) 3955–3967.
[11] S.K. Sinha, T. Sundararajan, V.K. Garg, A variable property analysis of alloy solidification using the anisotropic porous medium approach, Int. J. Heat Mass Transfer 35 (1992) 2865–2877.
[12] A.R. Chaudhuri, K.N. Seetharamu, T. Sundararajan, Modelling of steam surface condenser using finite element method, Comm. Num. Meth. Engng. 13 (1997) 909–921.
[13] S. Ergun, Fluid flow through packed column, Chemical Engineering Progress 48 (1952) 89–94.
[14] K. Vafai, S.J. Kim, On the limitations of the Brinkman–Forchheimer-extended Darcy equation, Int. J. Heat Fluid Flow 16 (1995) 11–15.
[15] B. Ramaswamy, T.C. Jue, J.E. Akin, Semi-implicit and explicit finite element schemes for coupled fluid/thermal problems, Int. J. Num. Meth. Engng. 34 (1992) 675–696.
[16] P. Nithiarasu, K.N. Seetharamu, T. Sundararajan, Double-diffusive natural convection in an enclosure filled with fluid saturated porous medium—a generalised non-Darcy

approach, Numerical Heat Transfer, Part A, 30 (1996) 413–426.

[17] A.J. Chorin, Numerical solution of Navier–Stokes equations, Math. Comp. 22 (1968) 745–762.

[18] E. David, G. Lauriat, P. Cheng, A numerical solution of variable porosity effects on natural convection in a packed-sphere cavity, ASME J. Heat Transfer 113 (1991) 391–399.